

LETTER

Generalized Mechanism for the Solid Phase Transition of M_2O_3 ($M=Al, Ga$) Featuring Single Cation Migration and Martensitic Lattice Transformation

Xiao Yang^a, Cheng Shang^{a,c*}, Zhi-Pan Liu^{a,b,c*}

a. Collaborative Innovation Center of Chemistry for Energy Materials (iChEM), Shanghai Key Laboratory of Molecular Catalysis and Innovative Materials, Key Laboratory of Computational Physical Science, Department of Chemistry, Fudan University, Shanghai 200433, China

b. Key Laboratory of Synthetic and Self-Assembly Chemistry for Organic Functional Molecules, Shanghai Institute of Organic Chemistry, Chinese Academy of Sciences, Shanghai 200032, China

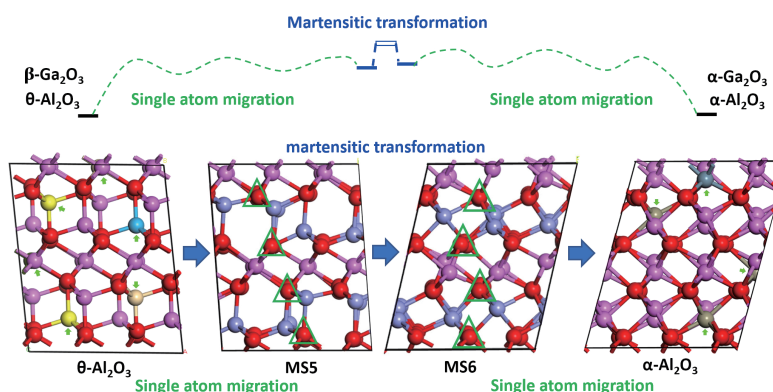
c. Shanghai Qi Zhi Institution, Shanghai 200030, China

(Dated: Received on April 18, 2024; Accepted on May 7, 2024)

Al_2O_3 and Ga_2O_3 exhibit numerous crystal phases with distinct stabilities and material properties. However, the phase transitions among those materials are typically undesirable in industrial applications, making it im-

perative to elucidate the transition mechanisms between these phases. The configurational similarities between Al_2O_3 and Ga_2O_3 allow for the replication of phase transition pathways between these materials. In this study, we investigate the potential phase transition pathway of alumina from the θ -phase to the α -phase using stochastic surface walking global optimization based on global neural network potentials, while extending an existing Ga_2O_3 phase transition path. Through this exploration, we identify a novel single-atom migration pseudo-martensitic mechanism, which combines martensitic transformation with single-atom diffusion. This discovery offers valuable insights for experimental endeavors aimed at stabilizing alumina in transitional phases.

Key words: Potential energy surface exploration, Neural network potential, Al_2O_3 , Ga_2O_3 , Solid-solid phase transition



Aluminum oxide (Al_2O_3) and Gallium oxide (Ga_2O_3) are both oxides of Group IIIA elements, with similar crystal phases at room temperature. The most stable crystal phase of Al_2O_3 is the hexagonal α -phase, with space group of $R\bar{3}C$ (#167) [1]. Its oxygen sublattice adopts hexagonal closest packing (hcp), with all Al

atoms occupying octahedral voids (Al_O). Besides the α -phase, there exist several metastable phases known as transition alumina, including γ , δ , θ , *etc.* [1], among which the monoclinic θ -phase with space group of $C2/m$ (#12) [2] is the thermodynamically most stable transitional phase. Unlike the α -phase, the oxygen sublattice of the θ -phase follows face-centered cubic (fcc) packing, with 50% of Al atoms filling tetrahedral voids (Al_T) and the remaining 50% filling octahedral voids. The θ -phase typically forms through the dehydration of Boehmite ($AlOOH$) at approximately 1300 K and transforms into

* Authors to whom correspondence should be addressed. E-mail: cshang@fudan.edu.cn, zpliu@fudan.edu.cn

the α -phase upon further heating to 1500 K [1]. Interestingly, both α -Al₂O₃ and θ -Al₂O₃ have analogous phases in Ga₂O₃, corresponding to α -Ga₂O₃ and β -Ga₂O₃, respectively. However, the monoclinic β -phase is the most stable phase of Ga₂O₃ under ambient conditions, undergoing transformation into α -Ga₂O₃ by applying pressure up to 6.5 GPa, accompanied by a 10% reduction in volume [3, 4]. The reverse transformation from α -phase to β -phase typically occurs upon heating to 600 °C [5]. Due to the structural similarity between the two oxides, they are often used in mixtures in catalysts and semiconductor materials [6, 7]. However, owing to the differing stability of similar crystal phases in the two oxides, phase transitions easily occur during usage, resulting in undesired changes in material properties [8, 9]. Therefore, understanding the phase transition mechanism of the two oxides holds significant value for their improved utilization in industry.

The investigation of the θ - α phase transition of Al₂O₃ is scarce, primarily due to the high preparation temperature, the presence of mixed crystal phases, and the rapid phase transition, making direct experimental observation challenging. Although the complete mechanism for this phase transition remains elusive, it has long been recognized that the contacts between the alumina particles dominate the sintering process [10]. Recently, through the preparation of rod-shaped θ -Al₂O₃ samples exposing different crystal facets, Jang *et al.* [11] discovered that the phase transition temperature (1500 K) of nanorods exposing the (110) surface is notably lower than that (1600 K) of nanorods exposing the (100) surface, suggesting anisotropic configurational evolution during the phase transition. Theoretically, Huang *et al.* [12] drew upon the “synchro-shear” mechanism that was proposed in 1963 by Kachi *et al.* [13], wherein the oxygen sublattice first undergoes layered slipping, transitioning from an fcc to an hcp motif, followed by the migration of Al atoms between adjacent octahedral voids. The pathway passes an intermediate state which is 0.53 eV/f.u. higher in energy than that of the θ -phase during the oxygen sublattice transformation from fcc to hcp. In comparison to Al₂O₃, significant effort has been devoted to understanding the phase transition from β -Ga₂O₃ to α -Ga₂O₃. Theoretically, Zhu *et al.* [14] discovered a multi-step mechanism through exploration of the global potential energy surface (PES), where the oxygen sublattice undergoes alternative hcp-fcc-hcp-fcc changes. The discovered orien-

tation relation (OR) is in good agreement with experimental observations. Subsequently, by further optimizing the intermediate states of this multi-step mechanism under 20 GPa, Song *et al.* [15] uncovered a new mechanism with an even lower energy barrier. This new mechanism requires only one hcp-fcc transformation and involves the overall migration of Ga atoms from tetrahedral voids to octahedral voids.

Considering the configurational similarity between Al₂O₃ and Ga₂O₃, here we have uncovered a comprehensive mechanism of the θ - α phase transition of Al₂O₃, which is built upon the low-energy Ga₂O₃ phase transition mechanism through extensive exploration of the global PES using a global neural network (G-NN) potential. Diverging from the phase transition mechanism found in Ga₂O₃, this novel mechanism revolves around the transition of Al atoms in fcc oxygen sublattice through a series of single-atom diffusions, rather than a one-step overall movement. The rate-determining step of this mechanism is a martensitic phase transformation, corresponding to the transition of the oxygen lattice from fcc to hcp phases.

All the pathway exploration of Al₂O₃ is performed using the SSW-RS method [16, 17], with global neural network potential [18] as implemented in LASP software [19, 20]. The transition states are located using VCDESW method [21]. The Al–O–H G-NN potential has a five-layer (269-80-80-80-5) feed-forward MBNN architecture for each element, in total containing 104895 fitting parameters, trained on a dataset containing energy, forces, and stresses of 13610 structures, which is calculated using plane-wave DFT calculations as implemented in VASP (Vienna *Ab-initio* Simulation Package) [22] with the following setups: the DFT functional being at the optB88-vdW functional level [23, 24], which showed good accuracy in computing the geometry and energies of several solid phase of alumina [25]; the kinetic energy cut off being 450 eV; the projector augmented wave (PAW) pseudopotential [26] utilized to describe ionic core electrons; the fully automatic Monkhorst-Pack K-mesh with 25 times the reciprocal lattice vectors [27] for the first Brillouin zone k -point sampling. To optimize the structure, we minimize the total energy until the total forces on each atom are smaller than 0.05 eV/Å. The root-mean-square errors (RMSE) for the energy and the force of the G-NN are 4.882 meV/atom and 0.177 eV/Å, respectively. The θ -phase model we employ comprises a 60-atom unit cell,

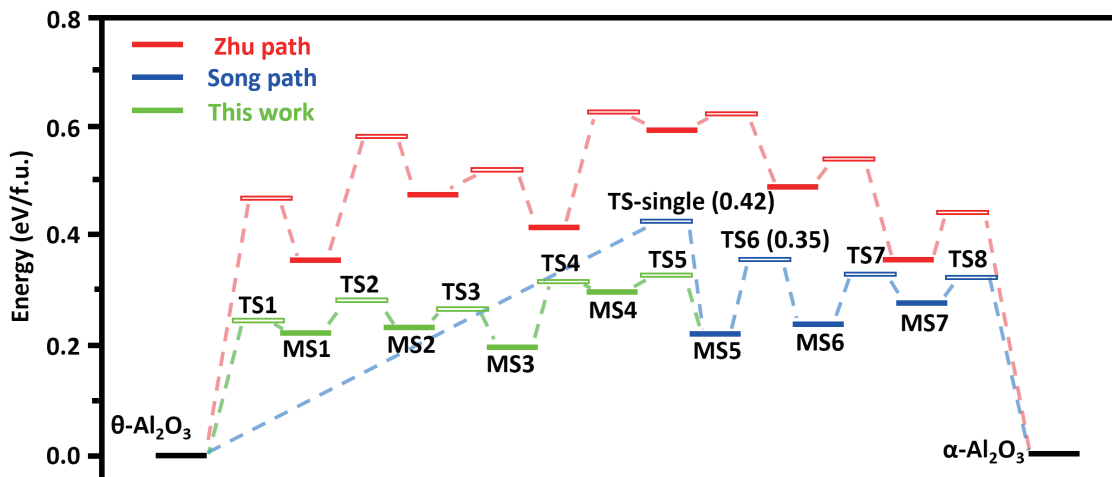


FIG. 1 The energy profile of three phase transition pathways from $\theta\text{-Al}_2\text{O}_3$ to $\alpha\text{-Al}_2\text{O}_3$. The path with red color is analog to the alternative fcc-hcp-fcc-hcp pathway as reported by Zhu *et al.* [14]. The blue path is analog to the single fcc-hcp transformation pathway as reported by Song *et al.* [15]. The green path is newly discovered in this work. The energy of the θ -phase is set to be zero. The transition states are represented by hollow bars and the intermediate states are shown by solid bars. The energies of the highest transition state of the single fcc-hcp path (TS-single) and the new path (TS6) are labeled in the figure.

analogous to the β -phase Ga_2O_3 model used in the previous literature [15]. All results reported in this work, including the energy profile of the phase transition pathway and the snapshots of configuration in Al_2O_3 and Ga_2O_3 , are finally converged using DFT calculations.

We firstly investigate the phase transition pathways following two mechanisms reported by Zhu *et al.* [14] and Song *et al.* [15] in Ga_2O_3 by substituting all the Ga atoms into Al in the intermediate states and locating the transition states. The energy profile is shown in FIG. 1. The energy of the θ -phase is set to be zero and the energy of $\alpha\text{-Al}_2\text{O}_3$ is 1.48 meV/atom. The barriers for both pathways are higher than those reported in Ga_2O_3 , aligning with the notably higher phase transition temperature in Al_2O_3 (1500 K) compared to Ga_2O_3 (900 K) [5]. The single fcc-hcp pathway (blue path in FIG. 1) still presents a lower energy barrier (0.42 eV/f.u.) than that (0.62 eV/f.u.) of the multiple fcc-hcp-fcc-hcp pathway (red path in FIG. 1). For the single fcc-hcp transition pathway, the transition state of the rate determining step is TS-single in FIG. 1, corresponding to the overall migration of Al atoms between several tetrahedral voids (Al_T) and octahedral voids (Al_O).

We then try to discover other possible transition pathways by using SSW-RS methods. The θ -phase, α -phase and all intermediate states in the single fcc-hcp pathways serve as the starting configuration for the

SSW-RS runs. For each starting configuration, we have performed 10000 SSW-RS runs, capturing structure pairs that connect the starting configuration with either α -phase or θ -phase. In total we have collected 87 pairs reaching α -phase and 2595 pairs reaching θ -phase. All those configuration pairs are then used to locate the transition states using DESW methods.

By analyzing all 2682 pathways, we indeed uncover a new pathway with a lower overall barrier than Song's mechanism. The key distinction between the two mechanisms lies in the transition pathway from the θ -phase to MS5. In this new pathway, depicted as the green path in FIG. 1, five elementary steps are involved. The highest energy along the path from θ -phase to MS5 corresponds to TS5, which is 0.10 eV/f.u. lower than the energy of TS-single. The remaining portion of the path, connecting MS5 with the α -phase, remains identical to the single fcc-hcp path, composed by a martensitic transformation step (MS5 to MS6) and two atomic diffusion steps (MS6 to α -phase) in sequence. As a result, the transition state of the rate determining step for the entire new pathway is now TS6, corresponding to an overall barrier of 0.35 eV/f.u., being much lower than that of the "synchro-shear" mechanism proposed by Huang *et al.* [12].

In FIG. 2(a), we present snapshots of the five elementary steps comprising the new path from the θ -phase to MS5, where each step involves local diffusion of one or two Al atoms. The first step involves two Al

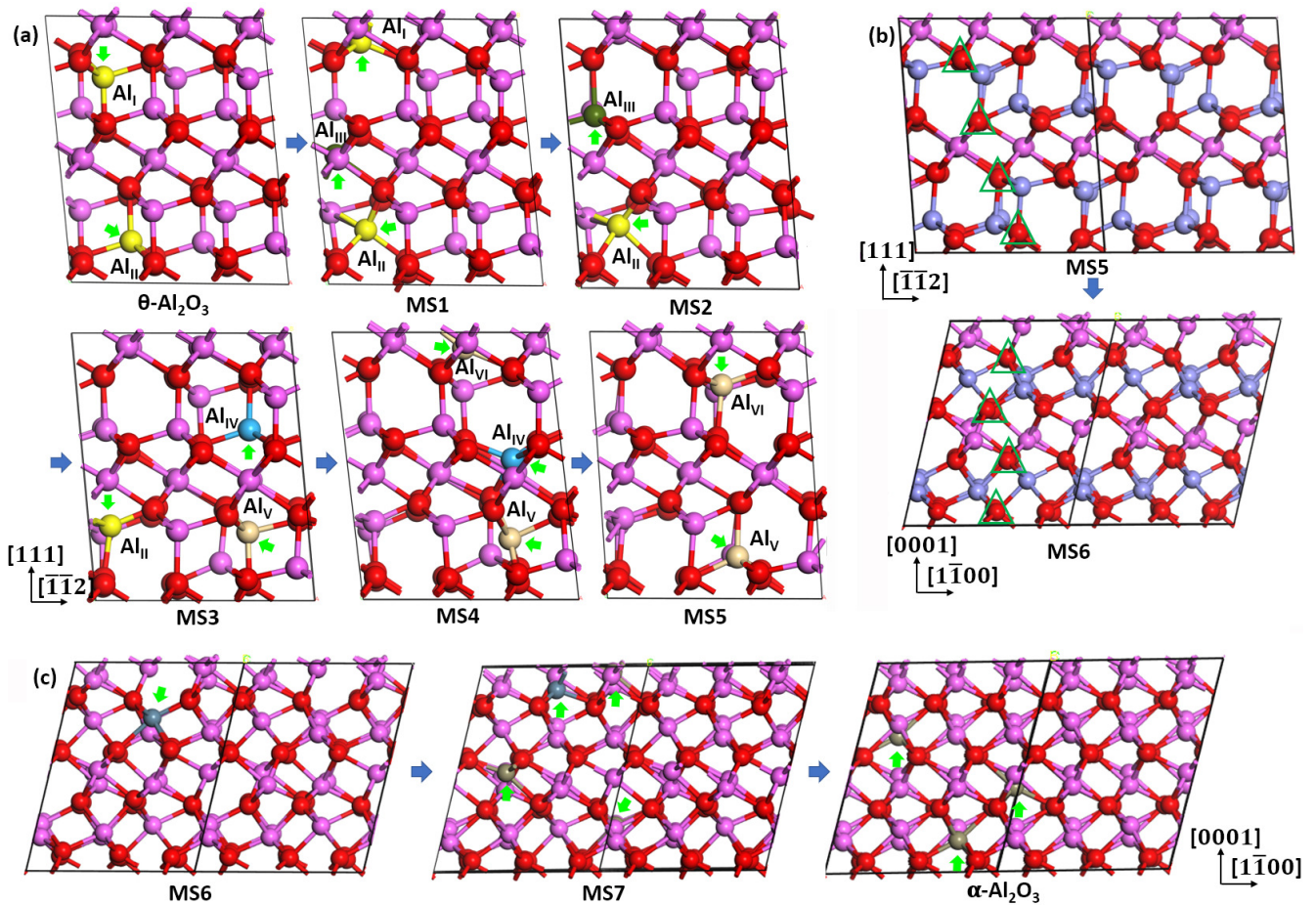


FIG. 2 (a) The snapshots of configurations along the θ - Al_2O_3 to α - Al_2O_3 transition pathway, corresponding to the green curve in FIG. 1. The migrating Al atoms of each step are highlighted by different colors and pointed by arrows. The lattice direction corresponding to the fcc sublattice is labeled. (b) The snapshots of MS5 and MS6 in FIG. 1. The Al atoms converting from Al_T to distort Al_O are highlighted in blue. Oxygen atoms in different closest packing plane are highlighted in green triangle for both configuration. (c) The snapshots of MS6, MS7 and α - Al_2O_3 . The migrating Al atoms of each step are highlighted by different colors and pointed by arrows. Purple, yellow, green, blue balls: Al, red balls: O.

moving from Al_T site to a nearby Al_O site along $[111]$ (Al_I) and $[11\bar{1}]$ (Al_{II}) direction, respectively. The second step involves Al_{III} moving from Al_O site to Al_T site along $[111]$ direction. The third step involves Al_{II} moving from Al_O site to Al_T site along $[11\bar{1}]$ direction. The fourth step involves Al_{IV} moving from Al_T site to a distort Al_O site along $[\bar{1}\bar{1}\bar{1}]$ direction and Al_V moving from Al_T to a distort Al_O site (five coordinated) along the $[00\bar{1}]$ direction. The fifth step involves Al_V moving from distort Al_O to the Al_T site along the $[00\bar{1}]$ direction and Al_{VI} moving from Al_T site to Al_O site along $[\bar{1}\bar{1}\bar{1}]$ direction. The transition distances of six Al atoms are all around 1.3 Å, corresponding to the distance between the nearest Al_T and Al_O site. Throughout the transition from the θ -phase to MS5, two Al_T atoms migrate to Al_O site, two Al_O atoms migrate to Al_T site and two Al_T atoms move to the adjacent Al_T sites, maintaining

the proportion of Al_T atoms at 50% in MS5. It is worth noting that the $\text{Al}_T \leftrightarrow \text{Al}_O$ migration of four Al atoms along $[111]$ and $[\bar{1}\bar{1}\bar{1}]$ all crossing the closest packing plane of oxygen sublattice, while for Al_{II} and Al_V , the migrating through Al_T - Al_O - Al_T path occurs between two oxygen closest packing planes. Notably, no lattice orientational change occurs during the whole process, and the oxygen sublattice retains the fcc close packing motif. However, due to the rearrangement of Al atoms, the lattice parameter shifts from ($a=8.41$ Å, $b=9.30$ Å, $c=8.41$ Å, $\alpha=87.62^\circ$, $\beta=116.70^\circ$, $\gamma=82.84^\circ$) in θ -phase to ($a=8.63$ Å, $b=9.25$ Å, $c=8.45$ Å, $\alpha=90.01^\circ$, $\beta=119.33^\circ$, $\gamma=83.08^\circ$) in MS5.

We have also shown the rate-determining step of MS5 to MS6 transition in FIG. 2(b), which is a martensitic transformation analogous to the corresponding pathway in Ga_2O_3 phase transition [15]. In this step,

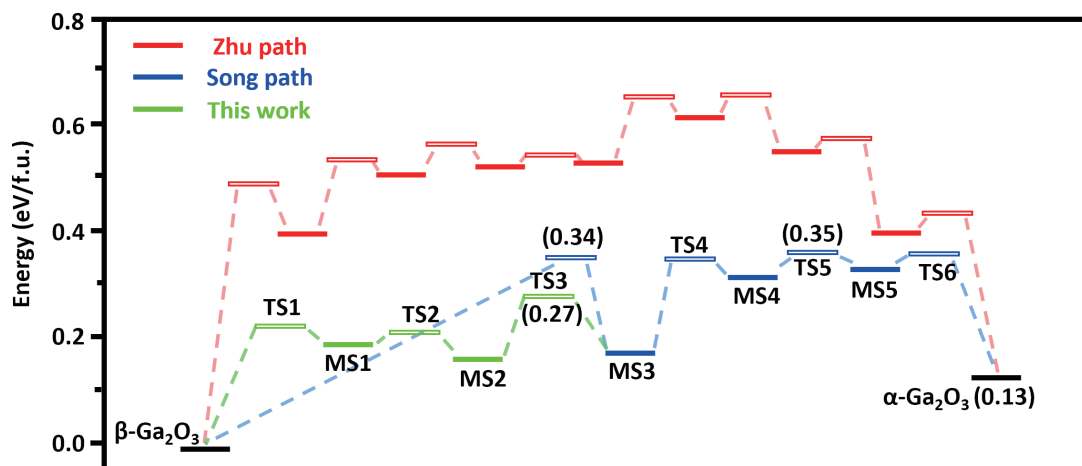


FIG. 3 The energy profile of three phase transition pathways from $\beta\text{-Ga}_2\text{O}_3$ to $\alpha\text{-Ga}_2\text{O}_3$. The red and blue path are reported by Zhu *et al.* [14] and Song *et al.* [15], respectively. The green path is newly discovered in this work. The energy of the β -phase is set to be zero. The transition states are represented by hollow bars and the intermediate states are shown by solid bars.

the fcc oxygen sublattice in MS5 transform into hcp motif in MS6 accompanied by the conversion of all Al_T atoms into distort Al_O atoms and an increase of density by 7.66%. The orientation relation (OR) in the hcp and fcc oxygen sublattice is $(0001)_{\text{hcp}}//(\bar{1}\bar{1}1)_{\text{fcc}}$ and $[11\bar{2}0]_{\text{hcp}}//[1\bar{1}0]_{\text{fcc}}$, indicating that the closest packing oxygen layer remains unchanged during the transition, as shown in FIG. 2(b). It is worth noting that the lattice parameters of MS5 in this step ($a=9.23 \text{ \AA}$, $b=8.43 \text{ \AA}$, $c=8.61 \text{ \AA}$, $\alpha=60.64^\circ$, $\beta=96.81^\circ$, $\gamma=90.01^\circ$) are different from that of MS5 in the step of MS4 to MS5. The final steps from MS6 to $\alpha\text{-Al}_2\text{O}_3$ involve four Al atoms migrating along $[0001]$ or $[000\bar{1}]$ direction (FIG. 2(c)), all crossing the closest packing oxygen plane, which are the same as those in Ga_2O_3 . This mechanism provides insights into the experimental observation that $\theta\text{-Al}_2\text{O}_3$ particles with exposure transforms into the α -phase at lower temperatures than samples primarily exposing the (100) surface [11]. We notice that the (110) surface of θ -phase corresponds to the $(111)_{\text{fcc}}$ surface, which is the habit plane of the martensitic transformation step in the lowest energy pathway. Hence by exposing more (110) surface, the α -phase is more likely to grow on this surface, triggering the phase transition of the contacted layers in θ -phase.

Finally, we examined the energy profile (FIG. 3) of the single-atom migration mechanism in the α -to- β phase transition of Ga_2O_3 . TS1–TS2 in FIG. 1 merges into TS1 in FIG. 3 and TS4–TS5 merges into TS3 in FIG. 3. The snapshots of Ga migration are shown in FIG. S1 (Supplementary materials, SM), where the Ga

atoms also show single atom movement. As shown in FIG. 3, our new mechanism indeed reduces the barrier from 0.34 eV/f.u. in Song's mechanism to 0.27 eV/f.u. for Ga atom migration in the fcc oxygen sublattice, indicating that the individual atom diffusion commonly exists in the oxygen fcc sublattice of Al_2O_3 and Ga_2O_3 and possibly other M_2O_3 metal oxide. However, the atom migration within the hcp oxygen sublattice remains the rate determining step.

In summary, by using the global PES exploration to extend the phase transition mechanism derived from Ga_2O_3 , we have unveiled a novel mechanism governing the phase transition between the θ -phase and α -phase of Al_2O_3 and the β -phase and α -phase of Ga_2O_3 . This new mechanism encompasses a combination of single atomic local diffusion and a martensitic transformation involving shearing of the oxygen sublattice parallel to the close packing plane, which we call single-atom pseudomartensitic transformation. The discovery of this mechanism provides potential guidance for the experimental synthesis of Ga_2O_3 and Al_2O_3 compounds with ideal phases and thermostabilities.

Supplementary materials: The computational detail of the training of Al–O–H ternary G-NN potential, the benchmark of G-NN potential against DFT calculations, the snapshots of Ga_2O_3 phase transition and the coordinates of key configurations are shown.

ACKNOWLEDGEMENTS

This work was supported by the National Natural

Science Foundation of China (No.12188101, No.22122301, No.22033003, No.91745201, No.91945301, No.92145302, and No.92061112), the Fundamental Research Funds for the Central Universities (20720220011), the National Key Research and Development Program of China (2018YFA0208600), and the Tencent Foundation for XPLOER PRIZE.

- [1] I. Levin and D. Brandon, *J. Am. Ceram. Soc.* **81**, 1995 (1998).
- [2] J. P. Remeika and M. Marezio, *Appl. Phys. Lett.* **8**, 87 (1966).
- [3] D. Machon, P. F. McMillan, B. Xu, and J. J. Dong, *Phys. Rev. B* **73**, 094125 (2006).
- [4] K. E. Lipinska-Kalita, B. Chen, M. B. Kruger, Y. Ohki, J. Murowchick, and E. P. Gogol, *Phys. Rev. B* **68**, 035209 (2003).
- [5] R. Roy, V. G. Hill, and E. F. Osborn, *J. Am. Chem. Soc.* **74**, 719 (1952).
- [6] M. Chen, J. Xu, F. Z. Su, Y. M. Liu, Y. Cao, H. Y. He, and K. N. Fan, *J. Catal.* **256**, 293 (2008).
- [7] H. Peelaers, J. B. Varley, J. S. Speck, and C. G. Van de Walle, *Appl. Phys. Lett.* **112**, 242101 (2018).
- [8] M. F. L. Johnson, *J. Catal.* **123**, 245 (1990).
- [9] K. Kaneko, K. Suzuki, Y. Ito, and S. Fujita, *J. Cryst. Growth* **436**, 150 (2016).
- [10] I. I. M. Tjibburg, H. De Bruin, P. A. Elberse, and J. W. Geus, *J. Mater. Sci.* **26**, 5945 (1991).
- [11] S. Jang, D. Gun Oh, H. Kim, K. Hyun Kim, K. Khivantsev, L. Kovarik, and J. Hun Kwak, *Angew. Chem. Int. Ed.* **63**, e202400270 (2024).
- [12] Y. C. Huang, X. Peng, and X. Q. Chen, *J. Alloys Compd.* **863**, 158666 (2021).
- [13] S. Kachi, K. Momiyama, and S. Shimizu, *J. Phys. Soc. Jpn.* **18**, 106 (1963).
- [14] S. C. Zhu, S. H. Guan, and Z. P. Liu, *Phys. Chem. Chem. Phys.* **18**, 18563 (2016).
- [15] W. L. Song, Y. P. Jia, S. L. Hu, and Z. P. Hu, *J. Phys. Chem. C* **124**, 23280 (2020).
- [16] C. Shang, X. J. Zhang, and Z. P. Liu, *Phys. Chem. Chem. Phys.* **16**, 17845 (2014).
- [17] X. J. Zhang and Z. P. Liu, *Phys. Chem. Chem. Phys.* **17**, 2757 (2015).
- [18] P. L. Kang, Z. X. Yang, C. Shang, and Z. P. Liu, *J. Chem. Theory Comput.* **19**, 7972 (2023).
- [19] S. D. Huang, C. Shang, P. L. Kang, X. J. Zhang, and Z. P. Liu, *WIREs Comput. Mol. Sci.* **9**, e1415 (2019).
- [20] P. L. Kang, C. Shang, and Z. P. Liu, *Chin. J. Chem. Phys.* **34**, 583 (2021).
- [21] X. J. Zhang and Z. P. Liu, *J. Chem. Theory Comput.* **11**, 4885 (2015).
- [22] G. Kresse and J. Furthmüller, *Comput. Mater. Sci.* **6**, 15 (1996).
- [23] M. Dion, H. Rydberg, E. Schröder, D. C. Langreth, and B. I. Lundqvist, *Phys. Rev. Lett.* **92**, 246401 (2004).
- [24] J. Klimeš, D. R. Bowler, and A. Michaelides, *J. Phys.: Condens. Matter* **22**, 022201 (2010).
- [25] H. van Gog, *Appl. Surf. Sci.* **541**, 148501 (2021).
- [26] G. Kresse and D. Joubert, *Phys. Rev. B* **59**, 1758 (1999).
- [27] H. J. Monkhorst and J. D. Pack, *Phys. Rev. B* **13**, 5188 (1976).